Structural and Membrane Binding Properties of the Prickle PET Domain[†]

Matthew Sweede,[‡,⊥] Gayatri Ankem,[‡,⊥] Boonta Chutvirasakul,[‡] Hugo F. Azurmendi,[‡] Souhad Chbeir,[‡] Justin Watkins,[‡] Richard F. Helm,[§] Carla V. Finkielstein,[||] and Daniel G. S. Capelluto*[,‡,||]

Departments of Chemistry, Biochemistry, and Biological Sciences, Virginia Polytechnic Institute and State University, Blacksburg, Virginia 24061

Received June 3, 2008; Revised Manuscript Received October 23, 2008

ABSTRACT: The planar cell polarity (PCP) pathway is required for fetal tissue morphogenesis as well as for maintenance of adult tissues in animals as diverse as fruit flies and mice. One of the key members of this pathway is Prickle (Pk), a protein that regulates cell movement through its association with the Dishevelled (Dsh) protein. Pk presents three LIM domains and a PET domain of unknown structure and function. Both the PET and LIM domains control membrane targeting of Dsh, which is necessary for Dsh function in the PCP pathway. Here, we show that the PET domain is monomeric and presents a nonglobular conformation with some properties of intrinsically disordered proteins. The PET domain adopts a helical conformation in the presence of 2,2,2-trifluoroethanol (TFE), a solvent known to stabilize hydrogen bonds within the polypeptide backbone, as analyzed by circular dichroism (CD) and NMR spectroscopy. Furthermore, we found that the conserved and single tryptophan residue in PET, Trp 536, moves to a more hydrophobic environment when accompanied with membrane penetration and that the protein becomes more helical in the presence of lipid micelles. The presence of LIM domains, downstream of PET, increases protein folding, thermostability, and tolerance to limited proteolysis. In addition, pull-down and tryptophan fluorescence analyses suggest that the LIM domains physically interact to regulate membrane penetration of the PET domain. The findings reported here favor a model where the PET domain is engaged in Pk membrane insertion, whereas the LIM domains modulate this function.

The noncanonical Wnt/planar cell polarity (PCP[1]) pathway mediates the establishment of cell polarity in the plane of epithelia in metazoans (*1*). In *Drosophila*, the effects of this signaling pathway can be observed in the distal orientation of wing hairs, the organization of a multifaceted eye, and the anterior-posterior orientation of bristles on the thorax, among others (*2*). A core of PCP signaling proteins, including Frizzled, Dishevelled (Dsh), Flamingo, Strabismus, Fat, Dachous, and Prickle (Pk) participate in tissue development in the *Drosophila* wing (*1*). The establishment of cell polarity involves a feedback amplification mechanism in which proximally localized Pk and Strabismus suppress Frizzled and Dsh on the proximal side, thereby facilitating the accumulation of Frizzled and Dsh on the distal side (*3*). These events promote the distal growth of the Actin hairs. To maintain this subcellular distribution, Pk physically interacts with Dsh at the plasma membrane (*3*). The *Drosophila prickle* gene encodes three isoforms (Pk, PkM, and Sple), which share three cysteine-rich, zinc finger-like LIM (Linl-1, Isl-1, and Mec-3) domains and a conserved PET (Prickle, Espinas, and Testin) domain, but they differ in the length of their N-terminal regions, and the balance among them is critical for the PCP in *Drosophila* imaginal disc development (*4*). Pk is expressed in mouse (*5*) and *Xenopus* (*6*) embryos in a dynamic pattern, which correlates with regions and cells involved in morphogenetic movements. This has led to the suggestion that the protein may serve a cytoskeletal scaffolding function. While LIM domains are protein interaction modules (*7, 8*), the function and structure of the PET domain is still unknown. Dsh presents three domains known as DIX, PDZ, and DEP, which have different roles in the multiple branches of the Wnt signaling pathway (*9*). The C-terminal region of Dsh, including its DEP domain, binds to Pk, whereas the PET-LIM region of Pk is necessary and sufficient for Dsh recognition (*3*). This interaction is thought to inhibit membrane targeting of Dsh, facilitating its accumulation at the distal side of the wing cells (*3*). Indeed, overexpression of Pk in zebrafish embryos inhibits Wnt/β-catenin signaling and increases the frequency of calcium transients (*10*), suggesting that Pk controls the equilibrium between the canonical and noncanonical Wnt pathway by regulating Dsh activity. Moreover, a Dsh-dependent downstream effector of the noncanonical Wnt pathway, c-jun kinase (JNK), is dramatically activated in a PET-LIM-dependent manner (*11*).

[†] This study was supported by grants from the Concern and Wendy Will Case Foundations and American Heart Association (to D.G.S.C.) and Susan G. Komen Foundation and American Heart Association (to C.V.F.).

* To whom correspondence should be addressed. Phone: 540-231-0974. Fax: 540-231-3255. E-mail: capellut@vt.edu.

[‡] Department of Chemistry.

[§] Department of Biochemistry.

[||] Department of Biological Sciences.

[⊥] These authors contributed equally to this work.

[1] Abbreviations: BS3, bis(sulfosuccinimidyl) suberate; CD, circular dichroism; DPC, dodecylphosphocholine; Dsh, Dishevelled; FPLC, fast performance liquid chromatography; HSQC, heteronuclear single quantum coherence; LIM, Linl-1 Isl-1 Mec-3; LMPC, lyso-myristoyl-phosphatidylcholine; LMPG, lyso-myristoyl-phosphatidylglycerol; MALDI, matrix assisted laser desorption/ionization; NMR, nuclear magnetic resonance, PET, Prickle Espinas Testin; Pk, Prickle; PCP, planar cell polarity; TFE, 2,2,2-trifluoroethanol.

10.1021/bi801037h CCC: $40.75
Published on Web 11/24/2008

Our study identifies for the first time the regions in Pk that are structurally and functionally relevant for membrane targeting. Size-exclusion chromatography, mass spectrometry, and cross-linking experiments as well as bioinformatics analyses establish that the PET domain is monomeric with a nonglobular conformation. Nuclear magnetic resonance (NMR), circular dichroism (CD), and limited proteolysis indicate that the Pk PET domain is poorly structured in solution. However, the addition of either 2,2,2-trifluoroethanol (TFE) or lipid micelles promoted an increment of the helical content in the PET domain, thus supporting the possibility of carrying out NMR-based structural studies of this membrane-binding domain. Fluorescence analysis shows that a single and conserved tryptophan residue in the PET domain exhibits a blue shift to a more hydrophobic environment accompanied with penetration in lipid micelles, suggesting a role of PET in Pk membrane targeting. Finally, the three LIM domains physically contact the PET domain, which favor the formation of a folded and stable interacting region, with the LIM domains providing a modulatory role in PET-mediated membrane penetration of Pk.

MATERIALS AND METHODS

Chemicals. The following is a list of chemicals used and their suppliers: TFE (Aldrich), dodecylphosphocholine (DPC) (Anatrace), lyso-myristoyl-phosphatidylcholine (LMPC) and lyso-myristoyl-phosphatidylglycerol (LMPG) (Avanti-Lipids), isopropyl β-D-thiogalactopyranoside (IPTG), bis(sulfosuccinimidyl) suberate (BS3), and 1,4 bismaleimidyl-2,3-dihydroxybutane (BMDB) (Pierce). All other chemicals were analytical reagent grade.

Cloning of Pk PET, PET-LIM, and LIM Modules. The *Drosophila* cDNA representing PET (amino acids 516−626 in Pk Sple), PET with the three LIM domains (PET-LIM; amino acids 516−809 in Pk Sple), and the three LIM domains (LIM123; amino acids 627−809 in Pk Sple) were cloned into a pGEX-6P-1 vector (GE HealthSciences). Primers used were as follows: 5′-CGCGGATCCGACATGCAGCGGCAGTCG-3′ (PET and PET-LIM, forward); 5′-CCGGAATTCCTAGCCGCGGCCCAGGGCATC-3′ (PET, reverse); 5′- CCGGAATTCCTACCCCTTGCTGCAGGCGATGGA-3′ (PET-LIM and LIM123, reverse) and 5′-CGCGGATCCTGCGACGACCTAATCTCCACG-3′(LIM123, forward). All constructs were confirmed by DNA sequencing.

Prediction of Disorder Propensity and Secondary Structure Content. The algorithms IUPRED (*12*) (http://iupred.enzim.hu/), PONDR (*13*) (http://www.pondr.com/) and GlobPlot (*14*) (http://globplot.embl.de/) were employed to predict the disorder propensity of the PET domain. The secondary structure content of the PET domain was predicted using PSIPRED (*15*) (http://bioinf.cs.ucl.ac.uk/psipred/psiform.html), JUFO (*16*) (http://www.meilerlab.org/view.php) and JPRED (*17*) (http://www.compbio.dundee.ac.uk/~www-jpred/). For each analysis, default program parameters were used.

Expression and Purification of Drosophila Pk Constructs. *Escherichia coli* cells, strain Rosetta (Novagen), were transformed with different Pk constructs. Five hundred milliliters of Luria−Bertani media was inoculated with an overnight preculture (1:50 dilution) and incubated at 37 °C until it reached an OD ≅0.8. Production of the protein was induced with 1 mM IPTG for 4 h at 25 °C. For PET-LIM and LIM123 expression, media were supplemented with 100 μM zinc sulfate. Uniformly ^{15}N-labeled PET was produced in M9 minimal media supplemented with $^{15}NH_4Cl$ (Cambridge Isotope Laboratories). Cells were pelleted and lysed by sonication in a solution containing 50 mM Tris-HCl (pH 7.3), 500 mM NaCl, 5 mM benzamidine, 0.1 mg/mL lysozyme, 5 mM dithiothreitol (DTT), and 0.5% Triton X-100. A supplement of zinc sulfate (100 μM) was added for PET-LIM and LIM123 purification. Crude extracts were centrifuged and the supernatant containing the fusion protein purified using glutathione affinity beads (GE HealthSciences) following manufacturer's instructions. Fusion proteins were digested with Prescission protease (60 Units/mL of beads) (GE HealthSciences) overnight at 4 °C. Untagged proteins were concentrated using standard concentrator devices (Millipore). Proteins were further purified by size-exclusion chromatography, and fractions containing the protein were pooled and concentrated for functional and structural analysis. The PET and PET-LIM domains were purified to homogeneity with yields of 3 and 0.5 mg/L of culture, respectively. The concentration of the proteins was estimated on the basis of their extinction coefficient calculated from the amino acid sequence and their absorbance values at 280 nm. Mass spectrometry (Virginia Tech Mass Spectrometry Incubator) and N-terminal sequencing (Tufts University Core Facility, Boston MA) verified the identity and integrity of the proteins.

Size-Exclusion Chromatography. The molecular mass of each of the Pk recombinant proteins was determined using size-exclusion chromatography. The purified PET domain was loaded onto FPLC using a Superdex 75 column (GE HealthSciences) in 50 mM Tris-HCl (pH 8) containing 250 mM NaCl and 1 mM DTT. The PET-LIM region was loaded onto a Superdex 200 column (GE HealthSciences) equilibrated with the buffer described above supplemented with 100 μM zinc sulfate. Protein standards for the Superdex 75 column were as follows: bovine serum albumin (BSA, 67 kDa), ovalbumin (OA, 45 kDa), carbonic anhydrase (CA, 29 kDa), chymotrypsinogen A (ChyC, 25 kDa), myoglobin (Myo, 17 kDa), and cytochrome *C* (CytC, 12.5 kDa). Standards for the Superdex 200 were tyroglobulin (Tyr, 669 kDa), ferritin (Fer, 440 kDa), catalase (Cat, 232 kDa), BSA, OA, and CA. Hydrodynamic radii of the proteins were calculated as reported (*18*).

Mass Spectrometry. For mass spectral analysis of the PET domain, the protein (~50 nM) in 20 mM ammonium acetate (pH 6.0) was mixed 1:1 with 10 mg/mL sinapinic acid (Aldrich) in 30:70 HPLC-grade acetonitrile/HPLC-grade water supplemented with 0.1% trifluoroacetic acid. A one-microliter aliquot was spotted onto a MALDI target plate and allowed to air-dry. The deposited sample was then analyzed in the linear positive ion-operating mode using an ABI 4800 MALDI TOF/TOF after calibration using the +1 and +2 peaks of apo-myoglobin.

Limited Proteolysis with Trypsin. Limited proteolysis of both PET and PET-LIM domains (5 μg each) were performed at room temperature from 1 to 60 min at a concentration of 0.1 μg/mL trypsin in 5 mM Tris-HCl (pH 6.8), 100 mM KF, and 0.1 mM DTT. Reactions were stopped by the addition of Laemmli buffer and analyzed by SDS−PAGE.

Chemical Cross-Linking. A chemical cross-linking reaction of the PET domain was performed in the presence of BS3

as described (*19*). Proteins (25 μM) were incubated with fresh BS3 (2.4 mM) in 100 mM HEPES (pH 7.5) for 1 h at room temperature. To test the effect of lipid micelles in the oligomeric state of the PET domain, 5 μg of the protein was incubated with LMPG, LMPC, and DPC at concentrations of 4, 0.3, and 3 mM, respectively, for 10 min at room temperature, and further cross-linking with BS3 was performed as described above. Cross-linking with BMDB (Pierce) was carried out according to the manufacturer's instructions. Reactions were stopped by the addition of Laemmli buffer and analyzed by SDS−PAGE.

Circular Dichroism Spectroscopy. Spectra were recorded on a Jasco J-815 spectropolarimeter. For acquisition of far-UV CD spectra, proteins (5 μM) in 5 mM Tris-HCl (pH 6.8), 100 mM KF, and 0.1 mM DTT were loaded in the absence or presence of either guanidine hydrochloride, DPC, LMPC, LMPG, or TFE. Experiments were carried out in a 1-mm path length quartz cell at room temperature. Spectra were obtained from five accumulated scans from 240 to 190 nm using a bandwidth of 1-nm and a response time of 1 s at a scan speed of 20 nm/min. Buffer backgrounds were used to subtract from the protein spectra. Spectra were deconvoluted to estimate secondary structure content with the online server DICHROWEB (*20*) using the CDSSTR algorithm (*21*). Near-UV CD spectra were collected using a 0.1-cm path length at 20 nm/min between 340 and 250 nm with a response time of 1 s and a data pitch of 0.5 nm. Because of the weak molar absorptivity of the aromatic amino acids, 30−60 μM of protein was employed for the near-UV CD experiments. Molar ellipticity was calculated using the Spectra Manager (Jasco) software. For thermal denaturation experiments, the temperature dependence of the ellipticity was followed at 222 nm, where the temperature was increased 1 °C/min, using a 1.5-nm bandwidth, an averaging time of 30 s and an equilibration time of 2 min.

NMR Spectroscopy. NMR samples contained 0.4 mM of the PET domain, 90%H_2O/10% ^2H_2O, 20 mM Tris-d_{11}-HCl (pH 6.8), 100 mM NaCl, 1 mM DTT-d_{10}, and 1 mM NaN_3. NMR experiments were performed at 25 °C on a Bruker Avance 600 MHz spectrometer equipped with triple detection standard probes with *z*-axis pulse field gradients (*22*). TFE titrations into the ^{15}N-labeled PET domain were analyzed by ^{1}H−^{15}N heteronuclear single quantum coherence (HSQC) experiments. Spectra were processed with NMRPipe (*23*) and analyzed using PIPP (*24*) and nmrDraw.

Fluorescence Spectroscopy. Intrinsic tryptophan fluorescence spectroscopy measurements were carried out using a J-815 Jasco spectropolarimeter at 23 °C in a 1-cm path length cuvette. The excitation wavelength was 295 nm, and the fluorescence emission spectra were recorded from 310 to 410 nm for each protein sample. The final concentration of the protein samples was between 0.3 and 0.6 μM. DPC (3 mM), LMPC (0.3 mM), and LMPG (4 mM) were added for protein−micelle interaction analyses. Quenching of tryptophan fluorescence in 5 mM Tris-HCl (pH 6.8) and 100 mM KF and 0.1 mM DTT was performed upon titration of acrylamide to 0.5 mM. The collisional quenching constant K_{sv} was determined using the Stern−Volmer constant:

$$F^\circ/F = K_{sv}[Q] + 1$$

where F° and F are the intensities of sample fluorescence in the absence and presence of the quencher, respectively, and [Q] is the molar concentration of the quencher (*25*).

Pull-Down Assay. A total of 5 μg of GST-LIM123-bound beads or an equivalent amount were incubated in binding buffer (20 mM Tris-HCl (pH 7.4), 100 mM NaCl, 0.1 mM DTT, and 0.1% Triton X-100) with 5 μg of purified PET domain in the absence and presence of 50 μM zinc sulfate for 2 h at room temperature. After washing the beads with low- and high-salt binding buffer (100 mM and 1 M NaCl, respectively), bound proteins were eluted in Laemmli sample buffer and analyzed by SDS−PAGE.

RESULTS

Cloning Strategy and Bioinformatics Analyses. We designed several GST-Pk fusion proteins containing the individual PET domain or a combination of the PET and LIM domains in order to characterize them structurally and functionally. The design of the PET domain ($PET_{516-626}$ defined in the text as PET) construct was based on its homology with other PET domains found in Pk-related proteins (Figure 1) (*4, 6, 26*) and by bioinformatics analyses (Figures 2A, B, and S1 (Supporting Information)). The prediction of the tertiary structure of the isolated PET domain was analyzed using three different algorithms (IUPRED, PONDR, and GlobPlot). These algorithms predicted the PET domain to be a relatively disordered protein with an average disorder propensity of 60, 57, and 70% using IUPRED, PONDR, and GlobPlot, respectively (Figure 2A). When IUPRED was used to analyze the tertiary structure of Pk, the disorder propensity of the PET domain was reduced, albeit still high (45%), with a propensity of order at the C-terminus near the LIM domains (Figure 2B). Native disordered proteins are extremely sensitive to proteolysis (*27*). Limited proteolysis of the purified PET domain with trypsin indicated that the protein was highly susceptible to proteolytic digestion (Figure 2C, top panel) since it was completely digested after one-minute incubation with the protease. Predictions of the secondary structure of the PET domain using PSIPRED, JUFO, and JPRED revealed the presence of four stretches of helical elements (Figure S1A, Supporting Information). When the PET domain was analyzed in the context of Pk using PSIPRED, the module exhibited three of the four predicted helical elements (the shortest is predicted to be absent in Pk) (Figure S1B, Supporting Information). Thus, predictions indicate that the secondary structural content of the PET domain does not significantly differ from the one obtained with the full-length protein. Combined with the limited proteolysis results, these data indicate that the PET domain likely presents a nonglobular tertiary disordered structure and that the PET domain boundaries indicated in Figure 1 can be considered as appropriate for structural and functional characterization studies. To understand whether the PET domain folds together with the LIM domains, a construct containing the three LIM domains (PET-$LIM_{516-809}$ defined in the text as PET-LIM) (Figure 1) was also designed. In contrast to the PET domain, the PET-LIM region appears to be relatively tolerant to limited proteolysis with trypsin (Figure 2C, bottom panel) suggesting that this region, presents a more compact structure, in agreement with our bioinformatics analysis (Figure 2B). Further support for our structural conclusions was obtained by characterizing the polypeptides produced by limited proteolysis of the

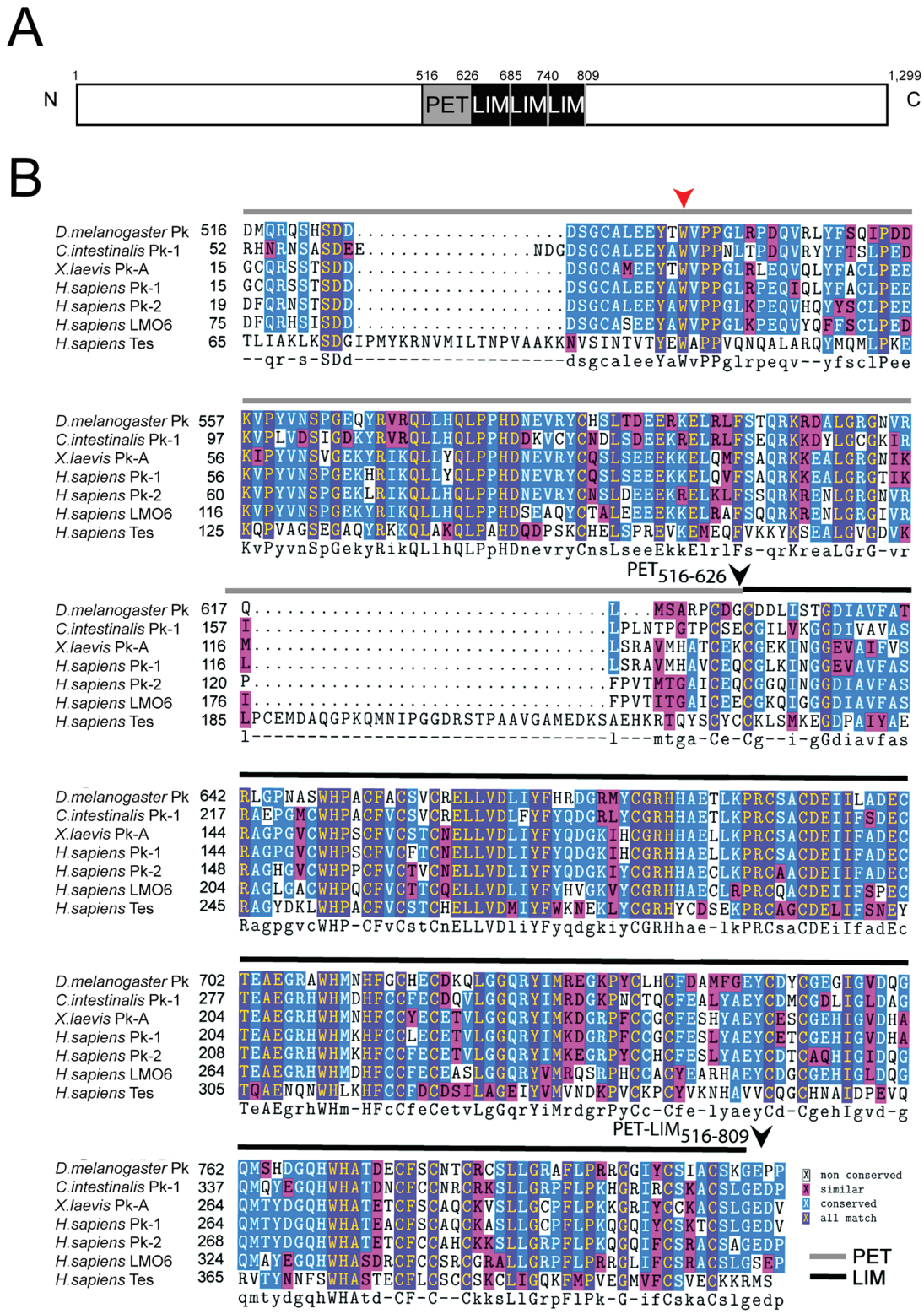

FIGURE 1: (A) Schematic representation of the *Drosophila* Pk primary structure with the boundaries of the PET and LIM domains indicated. (B) Amino acid sequence alignment of PET and LIM domains from Pk proteins found in different organisms. Residues are color-coded as indicated on the bottom right with the consensus sequence shown at the bottom of the aligned sequences. Boundaries of PET and LIM domains are indicated by bars on top of the sequences and are color-coded as shown at the bottom right. Black arrowheads represent the ends of the indicated constructs, and the red arrowhead indicates the Trp 536 residue in the PET domain. Sequences were aligned using the Molecular Biology Workbench Server.

Pk PET-LIM construct. A 5 min digestion with trypsin led to the formation of a slightly lower molecular weight polypeptide where ions for the N-terminus could not be detected (data not shown). Consistent with our structural predictions (Figure 2B), we confirmed the presence of a PET domain region sequence (LYFSQIPDDKV-PYVNSPGEQYR; amino acids 548−569 in Pk Sple) in all lower molecular weight protein bands indicated with asterisks (Figure 2C, bottom panel). These results suggest that the PET domain has limited access to trypsin,

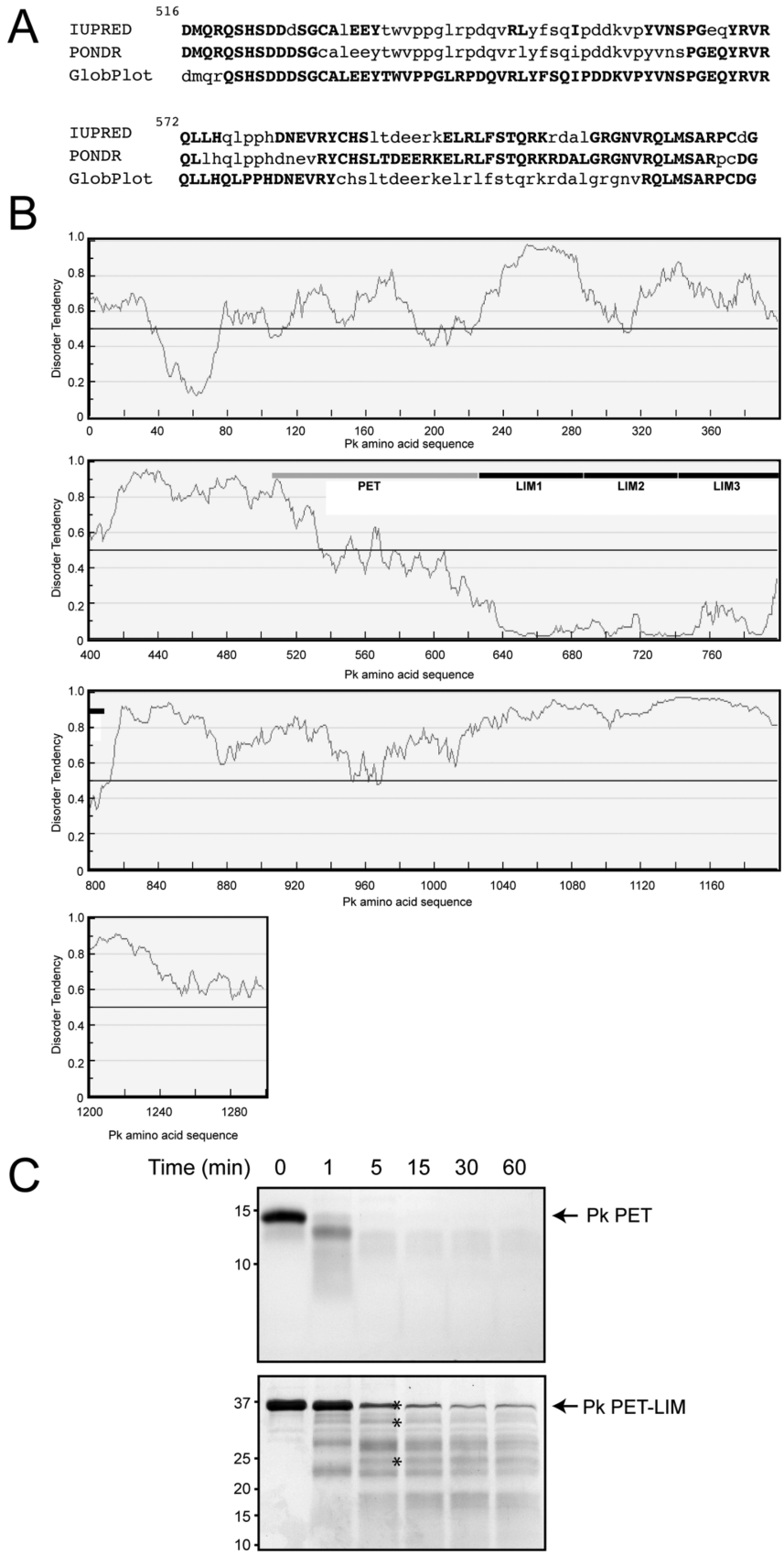

FIGURE 2: Structural analysis of the PET domain. (A) Disorder prediction analysis of the isolated PET domain was carried out using IUPRED, PONDR, and GlobPlot programs. Capital and lower case letters indicate disordered and ordered regions, respectively. (B) Disorder tendency of Pk was performed using IUPRED. The PET and LIM domains are shown as gray and black bars, respectively. Scores above 0.5 indicate disorder. (C) SDS−PAGE analysis of limited proteolysis of the PET domain (top panel) and PET-LIM modular region (bottom panel) at the indicated time points. Arrows indicate the starting protein material. Asterisks indicate trypsin-protected polypeptides analyzed by mass spectrometry and protein sequencing. Results are representative of a triplicate analysis.

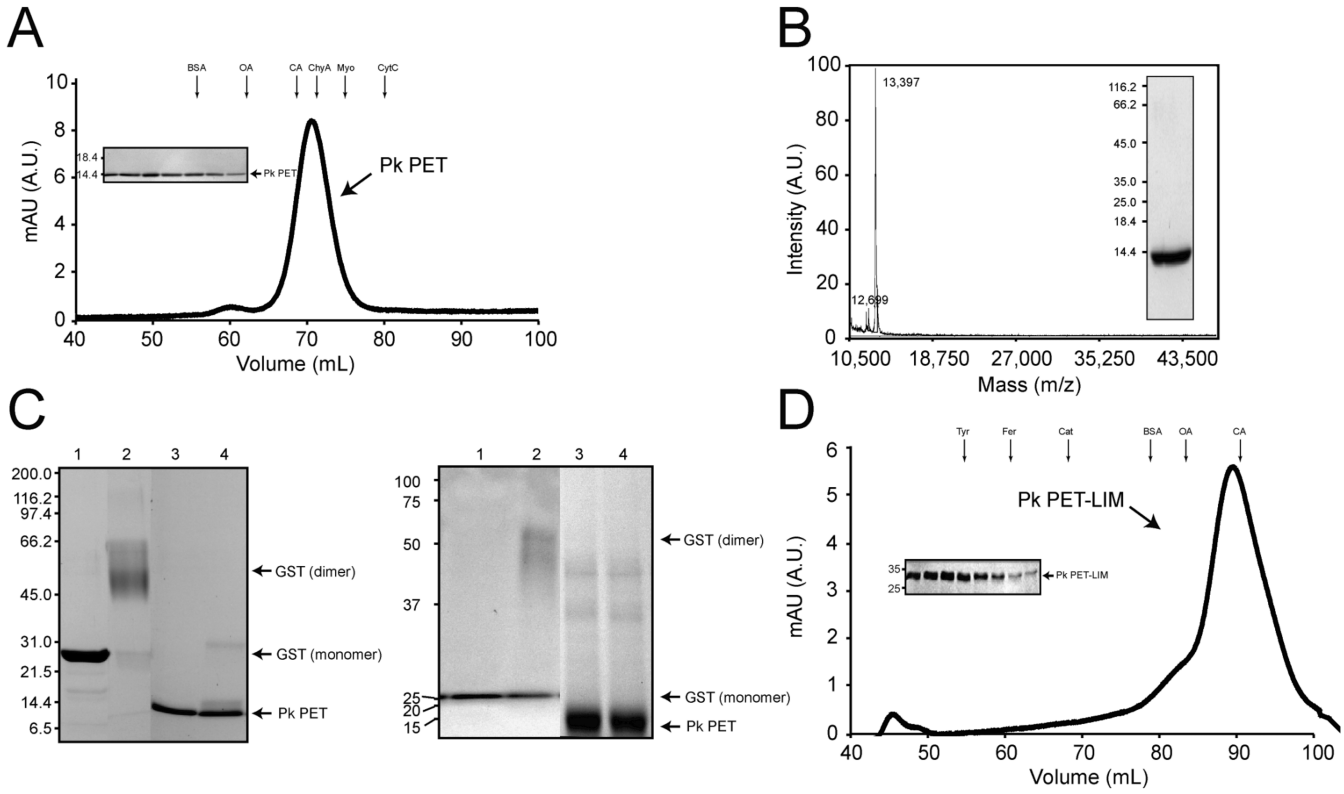

FIGURE 3: Oligomeric states of the PET and PET-LIM domains. (A) Size-exclusion chromatography (Superdex 75) of the purified Pk PET domain. Arrows show the elution volume of the indicated molecular weight markers. A.U.: arbitrary units. Inset: fractions corresponding to the elution peak were analyzed by SDS−PAGE. (B) Mass spectrum analysis of the PET domain. Inset: An SDS−PAGE gel of the PET domain. (C) Molecular cross-linking with BS3 (left) and BMDB (right) of the purified PET domain. Samples were resolved by SDS−PAGE. Lanes 1 and 2 are GST in the absence and presence of the cross-linker, respectively; lanes 3 and 4 are the PET domain in the absence and presence of cross-linker, respectively. Results similar to those presented were observed in three independent experiments. (D) Size-exclusion chromatography elution profile of purified Pk PET-LIM using a Superdex 200 column. The arrows show the elution of the indicated molecular weight protein markers. Inset: fractions corresponding to the elution peak were analyzed by SDS−PAGE.

supporting the proposal that the LIM domains provide protection to the PET domain.

Oligomeric States and Hydrodynamic Properties of Pk Domains. Size-exclusion chromatography was used to further purify both the PET and PET-LIM modules as well as establish their oligomeric states. Surprisingly, the PET domain (theoretical molecular mass of 13.4 kDa) elutes at a volume that corresponds to a 26.8 kDa globular protein (Figure 3A), thus closely resembles a dimer. We, therefore, estimated the hydrodynamic dimensions of the PET domain as a probe for elucidating the compactness of its tertiary structure (*18*). The corresponding calculated Stokes radius for an apparent mass of 26.8 kDa is 22.50 ± 0.49 Å. This value is larger than that calculated for a globular protein of 13.4 kDa (18.57 ± 0.09 Å), but significantly smaller than the same protein in an extended conformation (33.79 ± 0.01 Å). Furthermore, N-terminal sequencing and mass spectral analyses confirmed the identity of the protein and revealed a single prominent signal at 13,397 (Figure 3B and data not shown), closely resembling the estimated molecular mass of the PET domain. At least two possible scenarios explain these results: (i) the PET domain is monomeric, with a nonglobular and compact rather than extended conformation; (ii) the PET domain is a dimer, with labile noncovalent bonds playing a key role in maintaining its dimeric state in solution but not during mass spectral analyses. It should be noted, however, that the PET domain did not exhibit a protein peak corresponding to monomeric species at lower protein concentrations as expected for a monomer−dimer equilibrium when analyzed by size-exclusion chromatography (Figure 3A). Furthermore, the PET domain was incubated with BS3, a cross-linker reagent that covalently interacts with primary amines that are 11Å apart. Our result shows that the PET domain remained as a predominant ~13 kDa band after BS3 treatment and upon SDS−PAGE analysis, whereas GST, that is known to form dimers, exhibited a higher molecular weight band (~52 kDa) under the same experimental conditions (Figure 3C, left panel). Likewise, preincubation of the PET domain with the sulfhydryl-reactive cross-linker BMDB led to a single band on the gel that was indistinguishable from that observed with the untreated protein (Figure 3C, right panel). Overall, these results indicate that the PET domain is a monomer with a nonglobular tertiary structure. The presence of the three LIM domains at the C-terminus of the PET domain (PET-LIM; theoretical molecular mass of 34.0 kDa) shows a protein with a calculated molecular mass of 33.4 kDa from size-exclusion chromatography analysis (Figure 3D). This suggests that the PET-LIM region presents a globular and monomeric conformation, in agreement with our bioinformatics and limited proteolysis analyses (Figure 2).

Circular Dichroism Analysis. Next, we recorded CD spectra of the Pk PET domain to experimentally identify secondary structural elements in the protein. The CD spectrum shows a minimum at 205 nm and a positive signal at about 194 nm and below, suggesting that the protein is

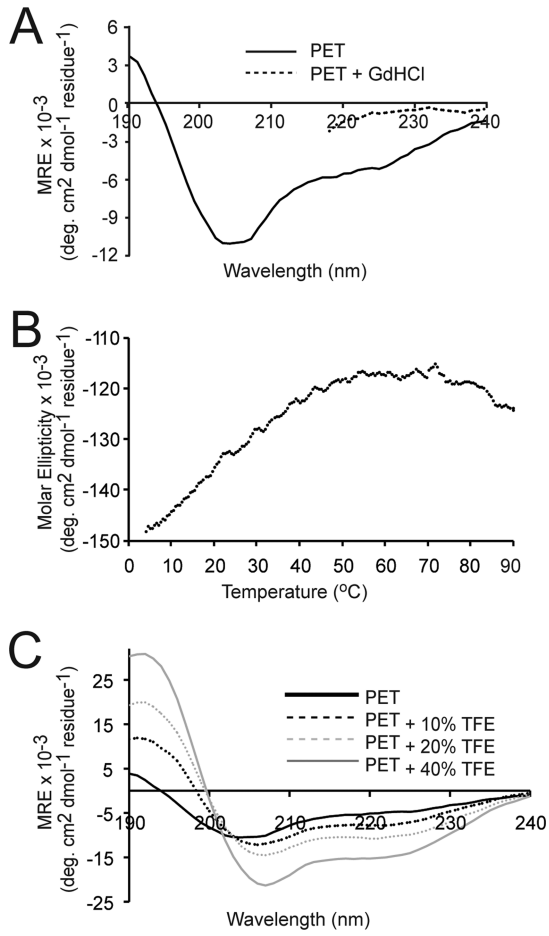

FIGURE 4: Far-UV CD analysis of the PET domain. (A) CD spectrum of PET domain (5 μM) in the absence and presence of 6 M guanidine hydrochloride. (B) Temperature-induced unfolding of the PET domain monitored by changes in ellipticity at 222 nm. (C) Effect of TFE on the CD spectrum of the PET domain. Concentrations of the cosolvent are indicated in the inset.

Table 1: Secondary Structure Analysis of the Pk PET (in the Absence and Presence of LMPG, LMPC, and DPC Micelles and TFE) and PET-LIM Constructs[a]

protein	αR	αD	βR	βD	turn	unordered	NRMSD	#valid solutions
PET	8	8	14	8	16	45	0.021	189
PET + LMPG	19	15	6	5	16	36	0.017	113
PET + LMPC	11	10	9	6	14	50	0.024	160
PET + DPC	14	11	9	6	14	46	0.019	162
PET + TFE	36	22	4	2	12	24	0.006	78
PET-LIM	15	13	13	9	21	29	0.014	255

[a] All values are in %. R and D represent regular and distorted secondary structure elements, respectively. NRMSD is the normalized root mean square difference of the experimental and calculated spectra.

poorly structured (Figure 4A). Deconvolution of the CD spectrum using CDSSTR indicated that PET consists of 8% α-helix, 14% β-sheet, and 45% random coil (Table 1). To confirm whether the PET domain presents secondary structure elements, the protein was incubated with 6 M guanidine hydrochloride resulting in a fully denaturated protein as reflected by the lack of a negative signal at 222 nm in its CD spectrum (Figure 4A). Thermal denaturation analysis revealed that the PET domain shows a continuous and gradual reduction in intensity of ellipticity when the sample temperature was raised from 4 to 80 °C without a precise transition at any temperature and with a reduction of

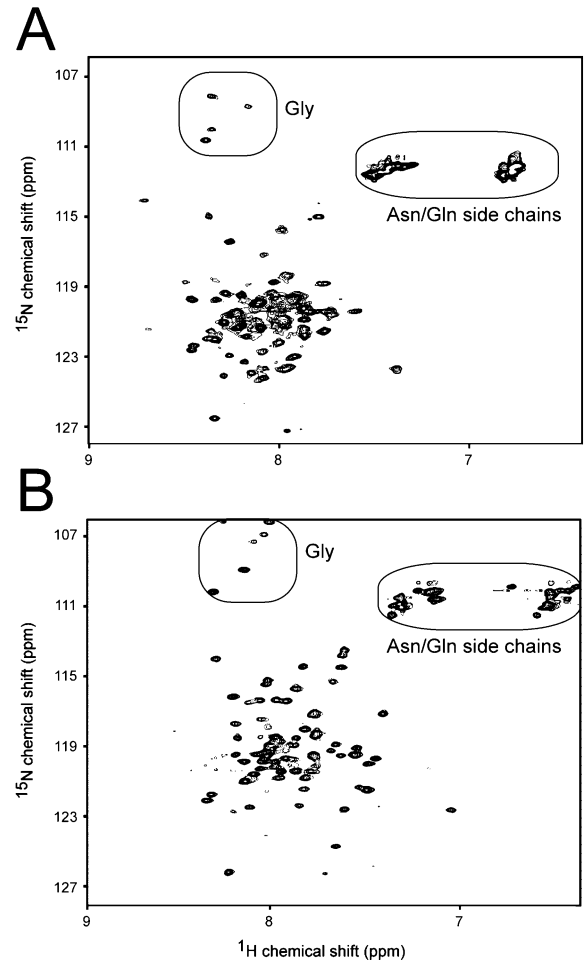

FIGURE 5: Two-dimensional ^{1}H−^{15}N HSQC NMR spectra of uniformly ^{15}N-labeled Pk PET domain (A) in the absence (B) and presence of 40% TFE. Resonances of potential glycine and side chains of asparagine and glutamine residues are boxed.

ellipticity from 80 to 90 °C (Figure 4B). This result is indicative of multiple secondary structural elements within the PET domain that, although contributing to the overall signal at 222 nm, melt at different temperatures. CD spectra of the PET domain recorded at increasing concentrations of TFE reveals a rise in its helical content as observed by the presence of a minimum at 208 and a shoulder at 222 nm (Figure 4C). Prediction of these secondary structural changes indicates a 36% of helical content of PET domain in the presence of 40% TFE (Table 1), close to the predicted secondary structure content (Figure S1, Supporting Information).

NMR Spectroscopy Analysis. The PET domain ^{1}H−^{15}N HSQC NMR spectrum shows a narrow dispersion of the backbone amide proton resonance signals and heterogeneous line widths (Figure 5A), indicating that the monomeric PET domain is poorly structured or dynamic, in agreement with our bioinformatics, limited proteolysis, and CD data (Figures 2 and 4, and Table 1). TFE is frequently used in NMR experiments of both proteins and peptides as it contributes to an increment of the α-helix and β-sheet contents by destabilizing hydrophobic interactions while reinforcing local hydrogen bonds within the polypeptide backbone (*28*). Addition of 40% TFE to the PET domain NMR sample improved both chemical shift dispersion (particularly in the NH dimension) and line width (Figure 5B). About 82% of

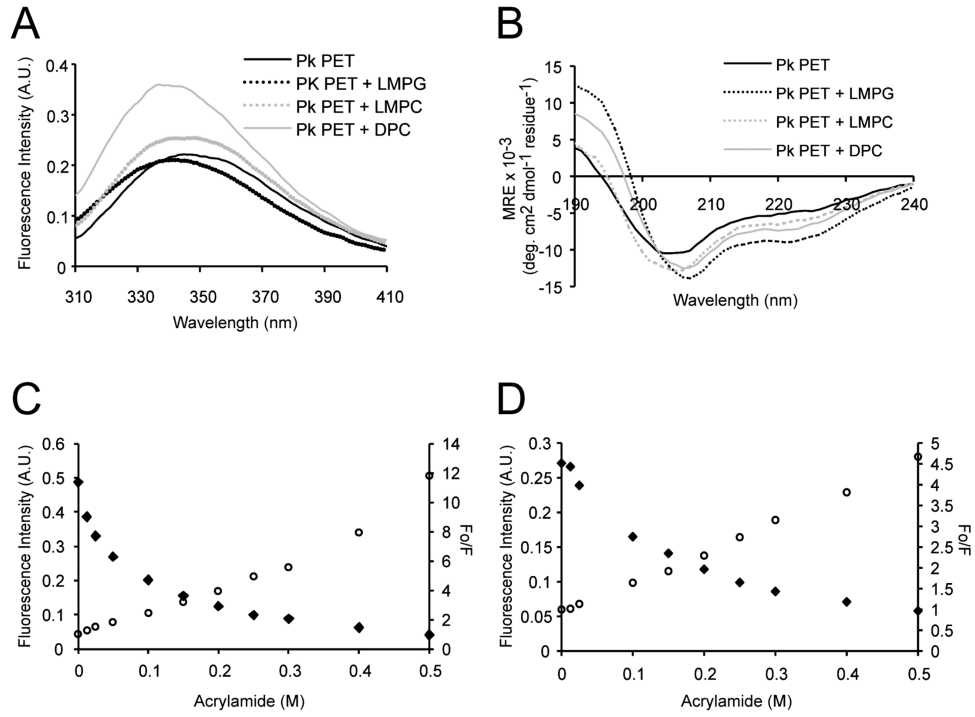

FIGURE 6: PET domain functional analysis. (A) Fluorescence emission spectrum of the Pk PET domain in the absence and presence of LMPG (4 mM), LMPC (0.3 mM), and DPC (3 mM) micelles as indicated in the inset. (B) Far-UV CD spectra of the PET domain in the absence and presence of LMPG (4 mM), LMPC (0.3 mM), and DPC (3 mM) micelles as indicated in the inset. (C) Stern-Volmer plot of the PET domain (0.6 μM) as a function of intermolecular acrylamide quenching. Quenching of PET fluorescence emission with acrylamide (◆) is shown together with a Stern-Volmer plot (○). (D) Same as (C), but the PET domain (0.3 μM) in the presence of LMPG micelles. Results similar to those presented in (C) and (D) were observed in three independent experiments.

the expected NHs as well as all 12 side chain resonances are detected under this condition. All six expected glycines (including the glycine translated from the vector) likely represent the glycine region of the NMR spectrum (Figure 5B). The Trp 536 NH indole is observed downfield in the spectrum in the absence and presence of TFE (data not shown). Some NMR signals still cannot be detected in HSQC experiments possibly due to local exchange broadening and/or rapid exchange of the amide protons with the solvent. Overall, the improved NMR spectrum suggests that the PET domain becomes more stabilized in the presence of TFE and that correlates with our CD structural analysis (Figure 4C).

Micelle Interactions and Acrylamide Quenching of the Pk PET Domain. The Pk PET domain presents a single conserved Trp (Trp 536; see Figure 1B, red arrowhead) that can be used to monitor structural changes in the protein. When excited at 295 nm, Trp 536 in the PET domain gives rise to an emission peak centered at 347 nm (Figure 6A), which is consistent with the Trp residue exposure into the aqueous solution. When the PET domain was incubated in the presence of DPC, LMPG, or LMPC micelles, the more hydrophobic environment and the decreased flexibility of the Trp residue caused a blue shift (Figure 6A), decreasing to 10, 5, and 6 nm in DPC, LMPC, and LMPG micelles, respectively. An increase in the fluorescence intensity was also observed when the PET domain was in either DPC or LMPC micelles, indicating that the Trp residue is buried in a hydrophobic environment. The Trp 536 blue shift in the presence of LMPG micelles is not as intense as other micelles, suggesting that this residue is less buried in the micelles. Addition of phospholipid micelles (DPC, LMPG, or LMPC) into the PET domain sample induced a red shift at the minimum and a more negative shoulder in the 215−230 nm region in the far-UV CD spectrum of the protein (Figure 6B), indicative of a conformational change in the PET domain in the presence of micelles. Deconvolution of the CD spectrum of PET in the presence of DPC, LMPC, and LMPG micelles resulted in an increment of helical structure concomitant with a reduction in the β-pleated sheet content of the protein (Table 1). This conformational change is not due to oligomerization since the PET domain remains monomeric in the presence of micelles after BS3 treatment (Figure S2, Supporting Information). Moreover, binding of PET to a more hydrophobic environment, such as to DPC micelles, does not change the thermal denaturation properties of the protein (Figure S3, Supporting Information), indicating that micelles do not promote a major change in the thermodynamic properties of the PET domain.

The relative exposure of a fluorophore to collisional quenching is measured by acrylamide quenching. Addition of acrylamide into a solution of the PET domain decreases the intensity of Trp fluorescence emission by 80% (Figure 6C), which resulted in a K_{sv} of 18.2 M^{-1}. This value is close to the iodide quenching of free tryptophan in solution (K_{sv} = 19.2 M^{-1}) (*29*), strongly suggesting the exposure of the conserved Trp 536 into the aqueous solution. The intrinsic fluorescence quenching exhibits a decreased K_{sv} value (8.43 M^{-1}) with increasing TFE concentration (Figure S4A), indicating increased inaccessibility of the Trp 536 residue to acrylamide. To determine the extent of the insertion of Trp 536 in the hydrophobic core of the micelles, fluorescence acrylamide quenching was also performed in the presence of LMPG and DPC micelles (Figures 6D and S4B). The effective K_{sv} value for the PET domain is of 7.50 and 10.36

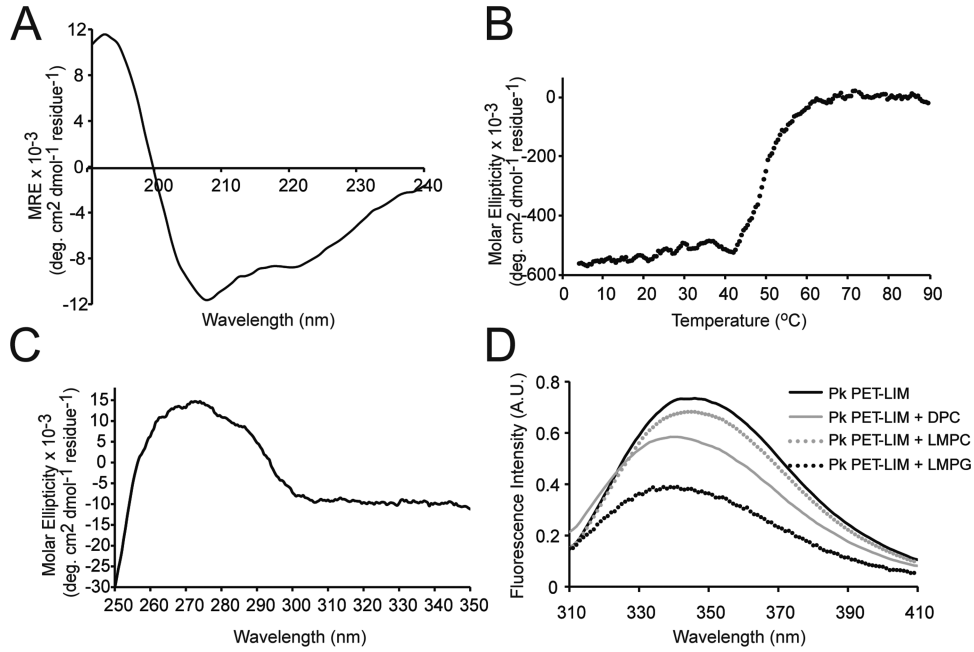

FIGURE 7: Structural analysis of the Pk PET-LIM region. (A) Far-UV CD spectra of the PET-LIM region (5 μM). (B) Thermal denaturation analysis of PET-LIM monitored by CD ellipticity at 222 nm. (C) Near-UV CD spectrum of PET-LIM (30 μM) at 23 °C. (D) Tryptophan fluorescence analysis of PET-LIM in the absence and presence of DPC (3 mM), LMPC (0.3 mM), and LMPG (4 mM) micelles.

M^{-1} for LMPG and DPC micelles, respectively, indicating Trp shielding due to PET domain insertion into micelles. Since the PET domain interacted with micelles, we asked whether the protein could interact with biologically relevant lipids found at the plasma membrane. In contrast to the observed phosphoinositide binding by the yeast Vam7p PX domain (*30*), neither PET nor PET-LIM were able to bind to the individual lipids tested by the protein−lipid overlay assay (Figure S5), suggesting that these modules require either a different lipid(s) or an organized membrane system for membrane targeting.

Structural Contribution of the LIM Domains in the PET-LIM Region of Pk. Next, we evaluated the contribution of the LIM domains in the secondary structure of PET-LIM using CD. The presence of three LIM domains increased the helical content of the protein showing a strong maximum at 193 nm, a minimum at 208, and a shoulder at 222 nm (Figure 7A and Table 1). We addressed PET-LIM structural stability by following its thermal denaturation at 222 nm (Figure 7B) in comparison with the PET domain (Figure 4B). The secondary structure of PET-LIM undergoes a cooperative thermal unfolding transition with a T_m of 50 °C. This result indicates that the PET-LIM region is not only tolerant to limited proteolysis (Figure 2C) but also relatively thermostable and thus suitable for further structural and functional studies.

To gain insight into the structural properties of PET-LIM, we carried out near-UV CD spectroscopy. Near-UV CD of proteins can be detected from the spatial organization of Trp, Tyr, and Phe side chains and, if present, disulfide bonds (*31*). Thus, near-UV CD signals are interpreted as an indication of a tertiary structure in the protein. Unlike the PET domain where near-UV CD signals are undetectable (data not shown), the spectrum of PET-LIM revealed negative bands between 285 and 350 nm presumably in part due to Trp side chain signals (Figure 7C). A positive and strong signal between 250 and 285 nm was also observed and likely due to the Phe side chains (Figure 7C). We next asked whether the LIM domains could influence PET micellar association. Quenching and a blue shift of the Trp fluorescence spectrum of the PET-LIM was observed in the presence of DPC, LMPC, and LMPG micelles (Figure 7D), suggesting that the Trp/s in the PET-LIM region contact micelles, but they are not deeply inserted, and rather, they localize in the proximity to the headgroup region of the micelles. To understand whether LIM domains regulate the PET domain by physical interaction, we performed a pull-down assay using GST-LIM123 bound beads. The PET domain directly interacted with the LIM domains only in the presence of zinc (Figure 8A), which is needed for correct folding of the LIM domains. This result suggests that the LIM domains modulate the function of the PET domain.

DISCUSSION

The PCP protein Pk is modular in nature containing a conserved PET domain followed by three LIM domains. The domain architecture and amino acid sequence homology of the conserved regions of Pk are also found in other human proteins such as Testin (Tes) and LMO6 (see Figure 1). Pk generates and maintains Frizzled localization and signaling on the distal and proximal sides of early pupal wing cells (*3*). Pk is usually cytosolic but localizes uniformly to membranes and subsequently becomes abundant on the proximal membranes, whereas Frizzled and Dsh are localized distally (*3*). To exert this function, the PET-LIM region of Pk interacts with the Dsh DEP domain (*3*). This interaction is believed to inhibit Dsh membrane localization and to antagonize signaling mediated by Frizzled on the proximal side of wing cells. Unlike *Drosophila* Pk, studies carried out with *Xenopus* Pk suggest that this protein cooperates with Dsh to activate JNK through its PET-LIM region (*11*). In either scenario, whether the PET and/or the LIM domains are necessary and sufficient to localize Pk at the membrane still remains unclear.

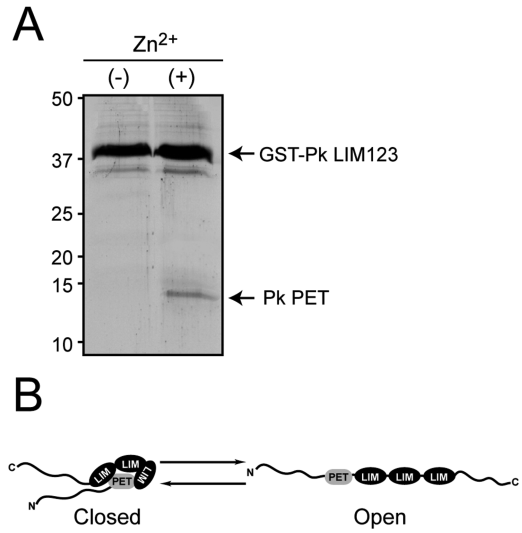

FIGURE 8: Interactions of the PET and LIM domains. (A) Recombinant GST-Pk LIM domain (LIM123)-bound beads were incubated with the PET domain in the absence and presence of zinc sulfate. The figure shown is representative of three experiments. (B) Proposed model showing the two putative conformational states of Pk.

The PET domain is a novel module that belongs to a small group of *pk*-related genes. No structural information is available for the PET domain, and therefore, its molecular function is still unknown. To dissect the function of the Pk domains, we functionally and structurally characterized the PET domain. This domain was calculated to be a dimer based on size-exclusion chromatography. However, further analysis utilizing mass spectrometry and chemical cross-linking as well as hydrodynamic calculations demonstrated that the PET domain is monomeric and that the elution of the protein by size-exclusion chromatography is due to a nonglobular three-dimensional shape (*32*).

Far-UV CD analysis of the PET domain indicates that the protein is relatively disordered with some secondary structural elements (Figures 4A and S1 (Supporting Information) and Table 1). Near-UV analysis of the PET domain revealed the absence of a globular tertiary structure in the protein (data not shown). The thermal denaturation curve obtained for the PET domain (Figure 4B) is likely a consequence of a sum of thermal-dependent structural changes in unstructured regions in combination with the melting of folded regions of the protein. This thermal-dependent unfolding behavior has also been recently observed in the human respiratory syncytial virus phosphoprotein (*33*). Further structural analysis of the PET domain by NMR spectroscopy confirmed our observations. The two-dimensional NMR spectrum exhibits poor resonance dispersion (Figure 5A) with some properties of an intrinsically disordered protein. Nonglobular conformations are commonly found in disordered protein domains that can well accommodate diverse target binding specificities in protein−protein interactions (*34*). They are generally found in proteins involved in the regulation of transcription and translation, signal transduction, protein phosphorylation, storage of small molecules, and the regulation of self-assembly protein complexes (*35*). Unfolded protein regions are characterized by a low content of buried hydrophobic residues as well as the presence of a high content of certain polar and charged residues (Gln, Ser, Pro, Glu, and Lys) (*35*) and indeed, the PET domain contains 34% of this class of charged and polar residues (Figure 1). Many intrinsically disordered protein domains experience transitions to more ordered states upon ligand binding. For example, the C-terminal transcription-activation domain of the hypoxia-inducible factor-1α is unstructured in the free state, but folds when bound to the cyclic-AMP-response-element-binding (CREB) protein (*36*). Similarly, the C-terminal segment of the archetypical Shaker Kv channel (ShB-C) is disordered (*37*). However, ShB-C is still able to bind its scaffold protein partner and mediates protein clustering *in vivo*, indicating that lack of structure is compatible with protein activity. On the basis of our structure prediction and limited proteolysis analyses, the PET domain likely exhibits disordered regions. However, the absence of a globular structure in the PET domain should not interfere with PET-dependent Pk interactions with physiological ligands.

Organic solvents, such as TFE, are often used to aid the formation of secondary structure in peptides and, in low concentrations, in proteins. High concentrations of TFE are also used as a denaturant in protein folding studies. The concentration of TFE that promotes destabilization over denaturation depends on the properties of the protein (*38*). Several reports indicate a correlation between helical propensity by TFE and primary sequence of the protein target (*39, 40*). TFE is proposed to favor hydrogen bonds and to inhibit hydrophobic interactions in proteins (*28*). This solvent has recently been used to structurally characterize the 18.5 kDa murine myelin basic protein (*41*) and the 7.7 kDa yeast aspartic proteinase inhibitor (*42*). We found that TFE promotes the helicity in the PET domain, in agreement with the secondary structure predictions, and likely disrupts hydrophobic interactions of the protein, as indicated by an increased number of NMR resonances and strong helical signals by CD, which were buried in the absence of the organic solvent. Thus, we propose that TFE favors the native conformation of the PET domain, and it is likely that this folded state is present when Pk is either bound to membranes or target proteins.

Since solvation effects from cosolvents, such as TFE, make it difficult to reach conclusions about the preferred conformation of the Pk PET domain at the cell membrane, other membrane-mimetic environments are better suited to approximate biological membranes. Many models have been used including detergent micelles, bicelles, and lipid bilayers (*43, 44*). Micelles are molecular aggregates formed in aqueous solution by amphipathic detergents at a critical concentration. Proteins or peptides can interact with membranes depending on the mode of their association and are usually classified as peripheral or integral. Peripheral proteins contact membranes through different moieties, whereas integral membrane proteins insert into the lipid bilayers. In either case, micelles facilitate their solubilization, and therefore, they are widely used for protein structural studies. Pk shuttles between the cytosol and membranes and, thus, can be considered as a peripheral membrane-binding protein. Membrane targeting of Pk is likely facilitated by its PET-LIM region (*3*). There is only one Trp residue (Trp 536) in the PET domain and its location can be inferred from tryptophan fluorescence studies. Results from these studies clearly indicate that the PET domain directly interacts with DPC, LMPG, and LMPC micelles (Figure 6), which are commonly used to mimic biological membranes (*43*).

Furthermore, from the Stern−Volmer calculations, we infer that the conserved Trp 536 inserts into the micelles and, thus, can be used to manipulate Pk subcellular localization and to understand the biological function of the PET domain. Micelles induce a helical conformation of the PET domain as observed from CD studies (Figure 6B). These conformational changes are similar in the presence of TFE, albeit the PET domain becomes more helical with alcohol. The differences between the PET domain secondary structural calculations in TFE and micelles can be attributed to the effects of alcohols on protein structures in which alcohols weaken nonlocal hydrophobic interactions, favoring local polar interactions such as hydrogen bonding (*45*).

The LIM domain is a cysteine-rich module with two zinc fingers, each containing two orthogonally packed antiparallel β-hairpins (*46*). In addition, the second zinc finger usually ends with a short helix (*46*). LIM domains are proposed to direct protein−protein interactions. They are found in a wide range of genes, and they display various functions including gene regulation and cell fate determination, tumor formation, and cytoskeleton organization (*47*). Likewise in SH2 domains, they are generally considered as adaptors. Despite the wealth of structural information about LIM domains, no discrete consensus binding sequence or structural elements have been identified (*46*).

Since three LIM domains are present downstream of the PET domain in Pk and because the entire PET-LIM region seems to be required for Pk to interact with Dsh at the membrane, we structurally analyzed this region. The presence of the three LIM domains downstream of the PET domain favored an increment of the secondary structure content in the PET-LIM region (Figure 7 and Table 1). In addition, the PET-LIM region displayed a tertiary structure in the near-UV region, with significant thermostability (Figure 7, panels B and C) and relative tolerance to trypsin-limited proteolysis (Figure 2C), thus making this construct appropriate for structural and functional studies. In addition and consistent with our bioinformatics analysis, the trypsin proteolysis studies indicated that the LIM domains protected a region of the PET domain comprising the amino acids 548−569 in Pk Sple. In contrast to the observed increment in fluorescence intensity observed for the PET domain, the PET-LIM multimodular region spectrum was quenched by the presence of lipid micelles. Since micelles also induced a blue shift of the fluorescence signal of PET-LIM, the overall data suggests that the LIM domains modulate the membrane penetration of the PET domain. However, we cannot exclude the possibility that other types of interactions between PET-LIM and micelles may occur; however, they do not involve Trp residues. Similar to our observations, the cytosolic C2A domain of synaptotagmin I controls membrane penetration of the adjacent C2B domain (*48*). Likewise, the intramolecular interaction between the SH3 domain and the PX domain in $p47^{phox}$ prevents nonspecific membrane penetration of the protein (*49*). Since we found that the LIM domains physically interact with the PET domain, we propose that the LIM domains intramolecularly modulate membrane penetration of the PET domain depending on the signal transmitted. In this regard, several models have been proposed for the mechanism of action of LIM domains (*46*). Among these, the LIM domains can contribute to protein function by promoting intramolecular interactions with proteins (*46*). Autoinhibitory LIM domains have been characterized in Tes, a Pk homologue. Tes is a putative tumor suppressor that contains an N-terminal PET domain and three C-terminal LIM domains. Garvalov et al. have shown that Tes binds to Actin, Mena, and vasodilator-stimulated phosphoprotein (VASP) (*50*). The authors revealed that the N-terminal region of Tes, containing the PET domain, binds to α-actinin and paxillin, in addition to Actin, whereas the C-terminal portion, containing the three LIM domains, recruits zyxin, in addition to Mena and VASP. Intriguingly, the N-terminal and C-terminal regions interact with each other *in vitro* and *in vivo* (*50*), and thus, this intramolecular association may preclude the docking of specific Tes partners. Similarly, autoinhibition of the LIM kinase by its LIM domain has been recognized by a deletion of the LIM domains or mutation of key zinc-coordinating residues that results in increased enzymatic activity (*51*). Therefore, on the basis of our results, we propose a mode of Pk regulation by switching from an open conformation state, where the PET and LIM domains do no interact, to a closed conformation state where the LIM domains modulate PET domain membrane penetration (Figure 8B), perhaps by interacting with residues 548−569 in the PET domain. Although further studies are needed to test this hypothetical model, it provides the basis to investigate the mechanism by which Pk is specifically targeted to the plasma membrane.

In summary, we have structurally and functionally characterized the Pk PET domain. We found that this conserved module is monomeric and nonglobular in nature, and is structurally stabilized by TFE and lipid micelles, thus making it a good candidate for NMR structural studies. Interestingly, its proposed role in membrane targeting is unmasked by lipid micelles studies, with the contiguous LIM domains likely exerting a regulatory function.

ACKNOWLEDGMENT

The *Drosophila* Prickle construct was a generous gift from Dr. Jeffrey Axelrod (Stanford University School of Medicine). We thank Dr. Keith Ray of the Virginia Tech Mass Spectrometry Incubator for performing the mass spectrometral analyses. We are also grateful to Katharine Howard for her contribution in the initial phase of this work.

SUPPORTING INFORMATION AVAILABLE

Secondary structure prediction of the PET domain (Figure S1), chemical cross-linking of the PET domain in the presence of micelles (Figure S2), thermal denaturation of the secondary structure of the PET domain in the presence of DPC micelles (Figure S3), acrylamide quenching of Pk PET domain in the presence of TFE and DPC micelles using tryptophan fluorescence (Figure S4), and protein−lipid overlay assay analysis of PET and PET-LIM domains (Figure S5). This material is available free of charge via the Internet at http://pubs.acs.org.

REFERENCES

1. Klein, T. J., and Mlodzik, M. (2005) Planar cell polarization: an emerging model points in the right direction. *Annu. Rev. Cell Dev. Biol 21*, 155–176.

2. Adler, P. N. (1992) The genetic control of tissue polarity in *Drosophila*. *BioEssays 14*, 735–741.
3. Tree, D. R., Shulman, J. M., Rousset, R., Scott, M. P., Gubb, D., and Axelrod, J. D. (2002) Prickle mediates feedback amplification to generate asymmetric planar cell polarity signaling. *Cell 109*, 371–381.
4. Gubb, D., Green, C., Huen, D., Coulson, D., Johnson, G., Tree, D., Collier, S., and Roote, J. (1999) The balance between isoforms of the Prickle LIM domain protein is critical for planar polarity in *Drosophila* imaginal discs. *Genes Dev. 13*, 2315–2327.
5. Bekman, E., and Henrique, D. (2002) Embryonic expression of three mouse genes with homology to the *Drosophila melanogaster* Prickle gene. *Gene Exp. Patterns 2*, 73–77.
6. Wallingford, J. B., Goto, T., Keller, R., and Harland, R. M. (2002) Cloning and expression of *Xenopus* Prickle, an orthologue of a *Drosophila* planar cell polarity gene. *Mech. Dev. 116*, 183–186.
7. Dawid, I. B., Breen, J. J., and Toyama, R. (1998) LIM domains: multiple roles as adapters and functional modifiers in protein interactions. *Trends Genet. 14*, 156–162.
8. Bach, I. (2000) The LIM domain: regulation by association. *Mech. Dev. 91*, 5–17.
9. Wallingford, J. B., and Habas, R. (2005) The developmental biology of Dishevelled: an enigmatic protein governing cell fate and cell polarity. *Development 132*, 4421–4436.
10. Veeman, M. T., Slusarski, D. C., Kaykas, A., Louie, S. H., and Moon, R. T. (2003) Zebrafish Prickle, a modulator of noncanonical Wnt/Fz signaling, regulates gastrulation movements. *Curr. Biol. 13*, 680–685.
11. Takeuchi, M., Nakabayashi, J., Sakaguchi, T., Yamamoto, T. S., Takahashi, H., Takeda, H., and Ueno, N. (2003) The Prickle-related gene in vertebrates is essential for gastrulation cell movements. *Curr. Biol. 13*, 674–679.
12. Dosztanyi, Z., Csizmok, V., Tompa, P., and Simon, I. (2005) IUPred: web server for the prediction of intrinsically unstructured regions of proteins based on estimated energy content. *Bioinformatics 21*, 3433–3434.
13. Romero, P., Obradovic, Z., Li, X., Garner, E. C., Brown, C. J., and Dunker, A. K. (2001) Sequence complexity of disordered protein. *Proteins 42*, 38–48.
14. Linding, R., Russell, R. B., Neduva, V., and Gibson, T. J. (2003) GlobPlot: Exploring protein sequences for globularity and disorder. *Nucleic Acids Res. 31*, 3701–3708.
15. McGuffin, L. J., Bryson, K., and Jones, D. T. (2000) The PSIPRED protein structure prediction server. *Bioinformatics 16*, 404–405.
16. Meiler, J., and Baker, D. (2003) Coupled prediction of protein secondary and tertiary structure. *Proc. Natl. Acad. Sci. U.S.A. 100*, 12105–12110.
17. Cuff, J. A., Clamp, M. E., Siddiqui, A. S., Finlay, M., and Barton, G. J. (1998) JPred: a consensus secondary structure prediction server. *Bioinformatics 14*, 892–893.
18. Uversky, V. N. (1993) Use of fast protein size-exclusion liquid chromatography to study the unfolding of proteins which denature through the molten globule. *Biochemistry 32*, 13288–13298.
19. Capelluto, D. G., Kutateladze, T. G., Habas, R., Finkielstein, C. V., He, X., and Overduin, M. (2002) The DIX domain targets Dishevelled to Actin stress fibres and vesicular membranes. *Nature 419*, 726–729.
20. Whitmore, L., and Wallace, B. A. (2004) DICHROWEB, an online server for protein secondary structure analyses from circular dichroism spectroscopic data. *Nucleic Acids Res. 32*, W668−673.
21. Sreerama, N., and Woody, R. W. (2004) Computation and analysis of protein circular dichroism spectra. *Methods Enzymol. 383*, 318–351.
22. Capelluto, D. G., and Overduin, M. (2005) Secondary structure, 1H, 13C and 15N resonance assignments and molecular interactions of the Dishevelled DIX domain. *J. Biochem. Mol. Biol. 38*, 243–247.
23. Delaglio, F., Grzesiek, S., Vuister, G. W., Zhu, G., Pfeifer, J., and Bax, A. (1995) NMRPipe - a multidimensional spectral processing system based on Unix pipes. *J. Biomol. NMR 6*, 277–293.
24. Garrett, D. S., Powers, R., Gronenborn, A. M., and Clore, G. M. (1991) A common-sense approach to peak picking in 2-dimensional, 3-dimensional, and 4-dimensional spectra using automatic computer-analysis of contour diagrams. *J. Magn. Reson. 95*, 214–220.
25. Eftink, M. R., and Ghiron, C. A. (1981) Fluorescence quenching studies with proteins. *Anal. Biochem. 114*, 199–227.
26. Katoh, M., and Katoh, M. (2003) Identification and characterization of human PRICKLE1 and PRICKLE2 genes as well as mouse Prickle1 and Prickle2 genes homologous to Drosophila tissue polarity gene prickle. *Int. J. Mol. Med. 11*, 249–256.
27. Tompa, P. (2002) Intrinsically unstructured proteins. *Trends Biochem. Sci. 27*, 527–533.
28. Buck, M. (1998) Trifluoroethanol and colleagues: cosolvents come of age. Recent studies with peptides and proteins. *Q. Rev. Biophys. 31*, 297–355.
29. Louzada, P. R., Sebollela, A., Scaramello, M. E., and Ferreira, S. T. (2003) Predissociated dimers and molten globule monomers in the equilibrium unfolding of yeast glutathione reductase. *Biophys. J. 85*, 3255–3261.
30. Yu, J. W., and Lemmon, M. A. (2001) All phox homology (PX) domains from *Saccharomyces cerevisiae* specifically recognize phosphatidylinositol 3-phosphate. *J. Biol. Chem. 276*, 44179–44184.
31. Kelly, S. M., Jess, T. J., and Price, N. C. (2005) How to study proteins by circular dichroism. *Biochim. Biophys. Acta 1751*, 119–139.
32. Crimmins, D. L. (2005) Human N-terminal proBNP is a monomer. *Clin. Chem. 51*, 1035–1038.
33. Llorente, M. T., Taylor, I. A., LopezVinas, E., GomezPuertas, P., Calder, L. J., GarciaBarreno, B., and Melero, J. A. (2008) Structural properties of the human respiratory syncytial virus P protein: Evidence for an elongated homotetrameric molecule that is the smallest orthologue within the family of paramyxovirus polymerase cofactors. *Proteins 72*, 946–958.
34. Dyson, H. J., and Wright, P. E. (2002) Coupling of folding and binding for unstructured proteins. *Curr. Opin. Struct. Biol. 12*, 54–60.
35. Dyson, H. J., and Wright, P. E. (2005) Intrinsically unstructured proteins and their functions. *Nat. Rev. Mol. Cell Biol. 6*, 197–208.
36. Dames, S. A., Martinez-Yamout, M., De Guzman, R. N., Dyson, H. J., and Wright, P. E. (2002) Structural basis for Hif-1 alpha/CBP recognition in the cellular hypoxic response. *Proc. Natl. Acad. Sci. U.S.A. 99*, 5271–5276.
37. Magidovich, E., Orr, I., Fass, D., Abdu, U., and Yifrach, O. (2007) Intrinsic disorder in the C-terminal domain of the Shaker voltage-activated K+ channel modulates its interaction with scaffold proteins. *Proc. Natl. Acad. Sci. U.S.A. 104*, 13022–13027.
38. Povey, J. F., Smales, C. M., Hassard, S. J., and Howard, M. J. (2007) Comparison of the effects of 2,2,2-trifluoroethanol on peptide and protein structure and function. *J. Struct. Biol. 157*, 329–338.
39. Jasanoff, A., and Fersht, A. R. (1994) Quantitative determination of helical propensities from trifluoroethanol titration curves. *Biochemistry 33*, 2129–2135.
40. Luidens, M. K., Figge, J., Breese, K., and Vajda, S. (1996) Predicted and trifluoroethanol-induced alpha-helicity of polypeptides. *Biopolymers 39*, 367–376.
41. Libich, D. S., and Harauz, G. (2008) Solution NMR and CD spectroscopy of an intrinsically disordered, peripheral membrane protein: evaluation of aqueous and membrane-mimetic solvent conditions for studying the conformational adaptability of the 18.5 kDa isoform of myelin basic protein (MBP). *Eur Biophys. J. 37*, 1015–1029.
42. Ganesh, O. K., Green, T. B., Edison, A. S., and Hagen, S. J. (2006) Characterizing the residue level folding of the intrinsically unstructured IA3. *Biochemistry 45*, 13585–13596.
43. Sanders, C. R., and Sonnichsen, F. (2006) Solution NMR of membrane proteins: practice and challenges. *Magn. Reson. Chem. 44*, S24−40.
44. Wang, G. (2008) NMR of membrane-associated peptides and proteins. *Curr. Protein Pept. Sci. 9*, 50–69.
45. Dathe, M., and Wieprecht, T. (1999) Structural features of helical antimicrobial peptides: their potential to modulate activity on model membranes and biological cells. *Biochim. Biophys. Acta 1462*, 71–87.
46. Kadrmas, J. L., and Beckerle, M. C. (2004) The LIM domain: from the cytoskeleton to the nucleus. *Nat. Rev. Mol. Cell Biol. 5*, 920–931.
47. Zheng, Q., and Zhao, Y. (2007) The diverse biofunctions of LIM domain proteins: determined by subcellular localization and protein-protein interaction. *Biol. Cell 99*, 489–502.
48. Bai, J., Wang, P., and Chapman, E. R. (2002) C2A activates a cryptic Ca(2+)-triggered membrane penetration activity within the C2B domain of synaptotagmin I. *Proc. Natl. Acad. Sci. U.S.A. 99*, 1665–1670.
49. Stahelin, R. V., Burian, A., Bruzik, K. S., Murray, D., and Cho, W. (2003) Membrane binding mechanisms of the PX domains of

NADPH oxidase p40phox and p47phox. *J. Biol. Chem. 278*, 14469–14479.
50. Garvalov, B. K., Higgins, T. E., Sutherland, J. D., Zettl, M., Scaplehorn, N., Kocher, T., Piddini, E., Griffiths, G., and Way, M. (2003) The conformational state of Tes regulates its zyxin-dependent recruitment to focal adhesions. *J. Cell Biol. 161*, 33–39.
51. Nagata, K., Ohashi, K., Yang, N., and Mizuno, K. (1999) The N-terminal LIM domain negatively regulates the kinase activity of LIM-kinase 1. *Biochem. J. 343 Pt 1*, 99–105.

BI801037H